Advances in the kinetic simulation of microwave absorption in an ECR thruster

IEPC-2017-361

Presented at the 35th International Electric Propulsion Conference
Georgia Institute of Technology • Atlanta, Georgia • USA
October 8 – 12, 2017

Paul-Quentin. Elias.[1]

ONERA-The French Aerospace Lab, 91120 Palaiseau, France

Abstract: The power absorption is a key feature in the overall performances of the ECRA thruster. This paper presents the recent work performed in the frame of the EU project MINOTOR to develop a kinetic model able to simulate the microwave absorption in the ECR source. First, the heating dynamic of a uniform plasma is studied using a 3D3V PIC simulation and compared to an semi-analytical model. Then, as a first step toward large scale simulation, a 1D model of the thruster has been developed to take into account the trapping of electron within a given magnetic field tube.

Nomenclature

ECR = Electron Cyclotron Resonance
EEDF = Electron Energy distribution function
PIC = Particle In Cell

I. Introduction

THE concept of quasi-neutral ECR thruster is currently being investigated as a way to provide a cathode-less and grid-less plasma thruster. Within the frame of the EU project MINOTOR, the implementation currently under study at Onera is called ECRA (Electron Cyclotron Resonance and Acceleration)[1]. It involves a coaxial opened chamber and a diverging static magnetic field, as shown in Figure 1. The coaxial chamber is connected to a micro-wave generator at 2.45 GHz. The magnetic field strength is adjusted such as the resonance condition ($B_{ECR} = 87.5\ mT$) is reached within the source.

This thruster is being investigated experimentally, using in particular direct thrust measurements, electron temperature measurements in the plume and Laser Induced Fluorescence. In addition, a global model has been developed to compute the global performance parameters of the thruster. Its results have been successfully compared to experiments [2]. However, while this approach yields very quickly global thruster parameters, it cannot reveal the details of the wave-plasma coupling, nor the actual plasma dynamic in the coaxial chamber.
In fact, the optimization of the thruster requires improving our understanding of several key issues.

The first one is the coupling of the electromagnetic power into the plasma in the resonance zone. The resonance in itself is a non-linear process which produces a non-isotropic electron distribution function. In the pressure ranges used in the thruster ($p \sim 10^{-3}$ mbar) and the electron energy ($T_e \sim 50$ eV) the electron mean free path is the order to tens of centimeters, which is greater than the source radius. Therefore we can expect the electron transport to be non-local and strongly affected by the confining B field and the ambipolar electric field.

[1] Research Scientist, Physics Department paul-quentin.elias@onera.fr

A second issue is the effect of the coaxial chamber walls. These floating walls can be made of a conductive or dielectric material. The type of material has an impact on the wall processes such as the secondary electron emission and also on the swirl currents inside the source. While the dielectric material can accumulate surface charge to balance the ion flux and the electron flux locally, the conductive boundary only requires that the global ion flux equate the global electron flux. Therefore swirl currents can appear in the source [3] and can impact the overall performance of the source.

The modeling required to capture and study these physical processes has to take into account kinetic and non-local effects. The particle-in-cell (PIC) methods are natural candidates to such a task. Very few works have tackled the modeling of ECR sources applied to Electric propulsion Recently Takao et al. have successfully modeled a miniature gridded ECR source at 4 GHz [4]. However, to our knowledge, in the context of EP the modeling of a device similar to ECRA has never been done, and this is what motivates the current study. One of the reasons for that is the size and electron number density involved in ECR devices make direct PIC simulations a formidable task. However, when observing the current trend in high-performance computing, we can speculate that such a task can be more manageable in the near future. In addition, 1D or 2D simulations are much more manageable and can still provide a wealth of information for the issues described above.

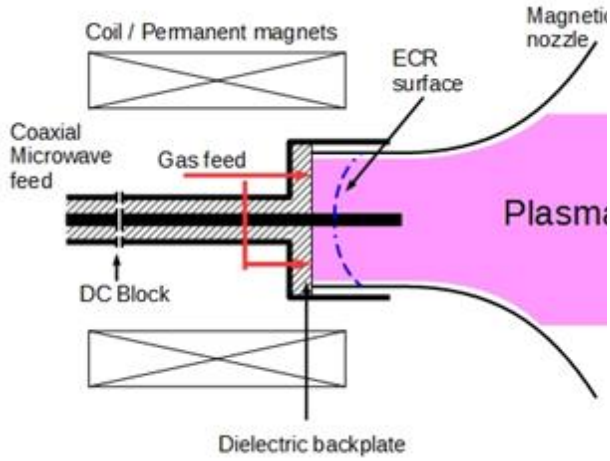

Figure 1. Schematic view of the ECRA thruster.

For these reasons, Onera is currently developing a new Particle-In-Cell/ Monte-Carlo Collision code adapted to the newly emerging massively parallel architectures. It aims modeling low-pressure plasmas produced in confined or semi-confined geometries, with arbitrary shape. The code dimensionality can be 1D3V, 2D3V or 3D3V. It uses a data hierarchy based on mesh blocks and tiles which enable either a pure MPI or a hybrid MPI/OpenMP parallelization[5]. For the simulation need of the ECR thruster, a dedicated electromagnetic solver is implemented. It needs to account for imbedded dielectric materials, and enforce absorbing boundary conditions at the thruster outlet. This work presents the steps toward the full-PIC modeling of the ECR thruster. First, a 1.5D model of the thruster is presented. This model includes several key physical processes (backplate charging, collisional processes, kinetic heating of the the plasma) that will be useful to improve our understanding of the thruster operation. It will also be used to guide the next steps in the thruster simulation, with the 2D and 3D version of the code. Second, an analysis of the microwave power absorption in the plasma is performed, and some preliminary results of the 1.5D model are presented.

II. 1.5D Model of the thruster

A. Constitutive equations

In order to study the basic heating mechanism in the ECRA thruster, a simplified kinetic model of the thruster has been defined and included in the 3D PIC code under development. The model considers the creation and expansion of a plasma in a magnetic field tube, as shown in Figure 2. All the plasma properties are considered constant along the section of the magnetic field tube but vary along its axis. The electrons and the ions are assumed to be confined within the magnetic field tube, whose area is related to the axial magnetic field intensity through

$$\frac{A(x)}{A_0} = \frac{B_0}{B_x(x)}$$

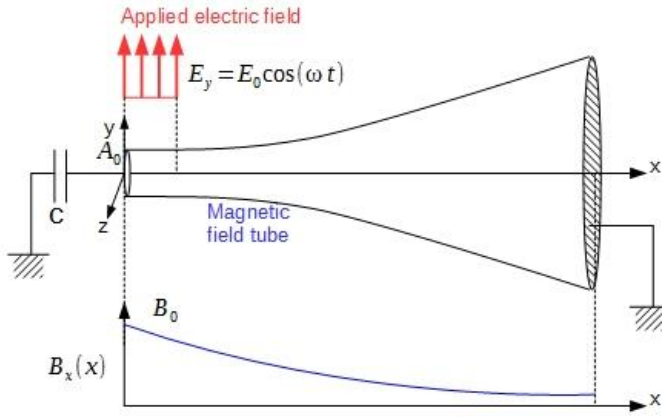

Figure 2. Principle of the 1.5D model. The plasma is assumed to be confined within an expanding magnetic field tube. The input power is modeled by a linearly polarized excitation (a standing wave pattern) in the source region that cover the leftmost part of the domain

We assume that the magnetic field is locally symmetrical along the field tube centerline. The field divergence is

$$\frac{1}{r}\frac{\partial(rB_r)}{\partial r} + \frac{\partial B_x}{\partial x} = 0$$

We assume that the magnetic field axial gradient depends on x only:

$$\frac{\partial B_x}{\partial x} = \alpha(x)$$

This means that B_x is constant along a section of the stream tube. Thus the radial component of the magnetic field is

$$B_z(r,x) = -\frac{\alpha(x)r}{2}$$

In this 1.5D model, the electron guiding center lies on the magnetic field tube centerline Ox. If $V_p = \sqrt{v_y^2 + v_z^2}$ is their transverse velocity, then the electron gyroradius is:

$$r_{L(x)} = \frac{V_p(x)}{\omega_C(x)}$$

As shown in Figure 3, the angle θ of the electron gyromotion in the transverse plane relates to the electron transverse velocity through:

$$\cos(\theta) = \frac{y}{r} = \frac{v_z}{V_p}$$

$$\sin(\theta) = \frac{z}{r} = -\frac{v_y}{V_p}$$

The magnetic field seen by the electron is simply

$$\vec{B} = \begin{cases} B_x(x) \\ B_y = B_r(r,x)\cos(\theta) \\ B_z = B_r(r,x)\sin(\theta) \end{cases}$$

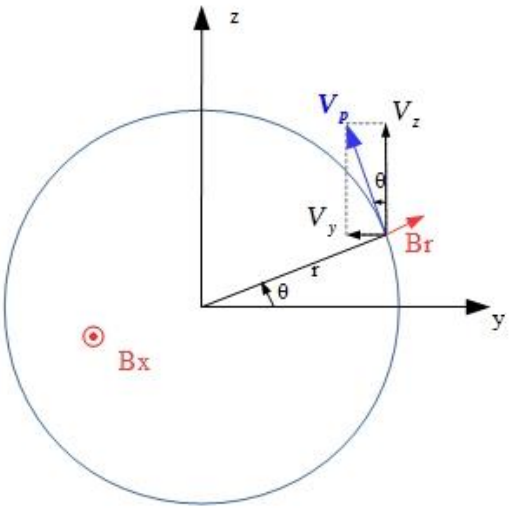

Figure 3. Cyclotron motion of the electron in the plane orthogonal to the magnetic field

With this expression for the magnetic field seen by the electron, it is possible to compute the Laplace force acting on the electron:

$$\vec{f} = -e\vec{v} \times \vec{B}$$

$$\begin{vmatrix} -ev_x \\ -ev_y \\ -ev_z \end{vmatrix} \times \begin{vmatrix} B_x \\ -\frac{\alpha v_z}{2\omega_c} \\ \frac{\alpha v_y}{2\omega_c} \end{vmatrix} = \begin{vmatrix} -\frac{e\alpha V_p^2}{2\omega_c} \\ \frac{ev_x v_y \alpha}{2\omega_c} - ev_z B\_x \\ \frac{ev_x v_z \alpha}{2\omega_c} + ev_y B_x \end{vmatrix}$$

It can be seen that the axial component of this for has the functional form:

$$f_x = -\mu\frac{\partial B_x}{\partial x}$$

Here, $\mu = \frac{\frac{1}{2}mV_p^2}{B_x}$ is the magnetic moment, and the force assume the classic "Grad B" form. Note that for this paraxial approximation to be valid, we must verify that

$$\frac{B_r}{B_x} \ll 1$$

This can be reformulated as

$$\frac{r_L}{L_B} \ll 1$$

With the following definition of the characteristic length for the magnetic field : $L_B(x) = \frac{B_x(x)}{dB_x/dx}$. For this model to remain valid, it is required that the electron Larmor radius remains much smaller than the characteristic variation length of the axial magnetic field.

B. Poisson equation

The one-dimensional particle pusher used in this study use the above form for the magnetic field. In addition, a Poisson equation couples the charge carried by the particles to the global field. In this model, we suppose that the electrostatic part of the electric field is aligned with the magnetic field. Thus, because of the varying section of the magnetic field tube, the Poisson equation is modified:

$$\epsilon_0 \frac{\partial}{\partial x}\left(\frac{B_0}{B(x)} E_x\right) = \frac{B_0}{B(x)}\rho$$

Or

$$\epsilon_0 \frac{d^2\phi}{dx^2} - \epsilon_0 \frac{1}{L_B(x)}\frac{d\phi}{dx} = -\rho$$

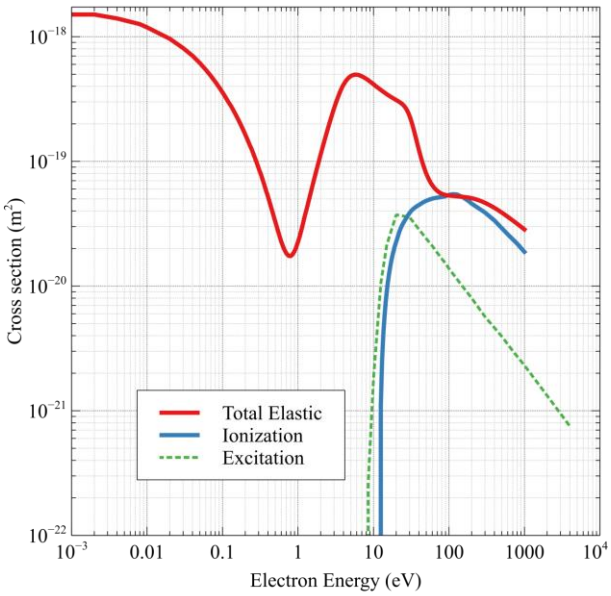

Figure 4. Total Elastic, Ionization and Excitation cross section of Xenon neutral by electron impact

To model the plasma heating by the microwaves, we consider that the TEM wave launched in the coaxial part of the thruster (see Figure 1) are reflected on the open end of the coaxial with negligible absorption. This results in a standing wave pattern in the coaxial cavity:

$$E_y = 2E_0 \cos(\omega t) \cos\left(\frac{2\pi(L-x)}{\lambda}\right) \quad x \in [0, L]$$

Since the source length L is much smaller than the microwave wavelength (2cm vs 12.5 cm), we simplify the above expression as

$$E_y = 2E_0 \cos(\omega t)$$

C. Collisions

The ECRA thruster uses mainly Xenon as a propellant.

We consider the total elastic collision cross section from McEachran[6], and ionization and excitation cross section provided by the Kinema database referenced in LXCAT[7]. Figure 4 shows the cross section used in the simulations.

D. Boundary conditions

The backplate of the thruster is made of a dielectric material (see Figure 1). This is modeled by setting the voltage on the backplate to that of an equivalent charged capacitor. The deposition of charges on the plasma exposed dielectric surface change the surface voltage $V_{BP}$of the dielectric backplate as the deposition of charge on a capacitor electrode change its voltage:

$$\Delta V_{BP} = \frac{\Delta Q}{\Delta t}\frac{1}{C}$$

The vacuum side of the thruster is supposed to be grounded, giving a Dirichlet condition for the Poisson equation.

For the particles, the backplate is considered a loss surface for the electrons and a surface able to emit secondary electrons for the ions. The ion-induced secondary emission coefficient γ is supposed to constant. The vacuum side boundary condition is a loss surface for both populations.

Finally, radial losses are modeled by discarding a fraction of the electrons that collide elastically with the background. This fraction depends on the Larmor radius after the collision. This models the fact that elastic

collisions lead to a random diffusion of the guiding center of the electrons that can leave the stream tube. For each electron thus removed an ion is also removed of the computational domain (close to the lost electron) to model the ambipolar field that accelerates ions toward the radial wall.

E. Numerical implementation

The above model is implemented as a module of a larger PIC/MCC code that is being developed at Onera for low-pressure plasma simulation. The code can run in serial or on massively parallel architecture. Here we briefly describe the main steps of the PIC code: the particle pusher, the charge deposit, the Poisson solver and the Monte-Carlo collisions module.

The particle pusher uses the classic 2nd-order accurate Boris scheme[8], using the three components of the magnetic field given above. The three components of the velocity are updated, taking into account the three components of the B field and the three components of the electric field. Finally the particle axial position is updated considering the axial velocity only. The radial position of the particle can be derived from the transverse velocity components.

The charge and current contribution carried by the particles is deposited using a linear interpolation. The charge and the boundary conditions are used by a parallel multigrid Poisson solver[9] to compute the potential and the electrostatic contribution to the electric field.

Finally, the Monte-Carlo module can handle several background gases and an arbitrary number of collisional processes. The null collision technique is used to speed up the sorting between colliding and non-colliding particles. Coulomb collisions are not considered in this work because the plasma density is low.

The code uses a 2-level parallelism, using MPI and/or OpenMP. The simulation done in this study have been done using a 4-cores workstation.

F. Validation: Magnetic Mirror

As a test for the 1.5D model, we consider the case of the magnetic mirror. A maxwellian electron population is injected in a magnetic bottle as shown in Figure 5. As expected, the fraction of the population in the loss cone is lost to the wall, while the other electrons remain confined. In Figure 6, we verify that the loss cone angle is :

$$\sin^{-1}(\theta) = \frac{B_{min}}{B_{max}}$$

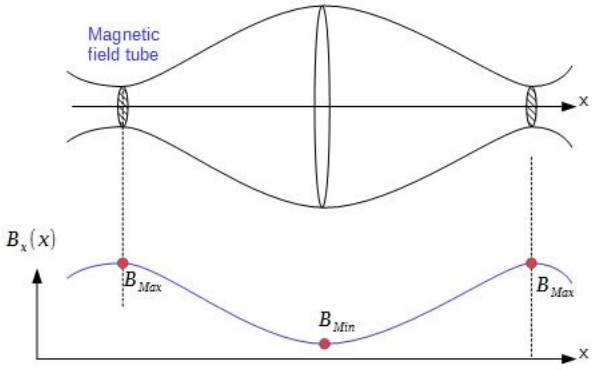

Figure 5. Magnetic mirror configuration

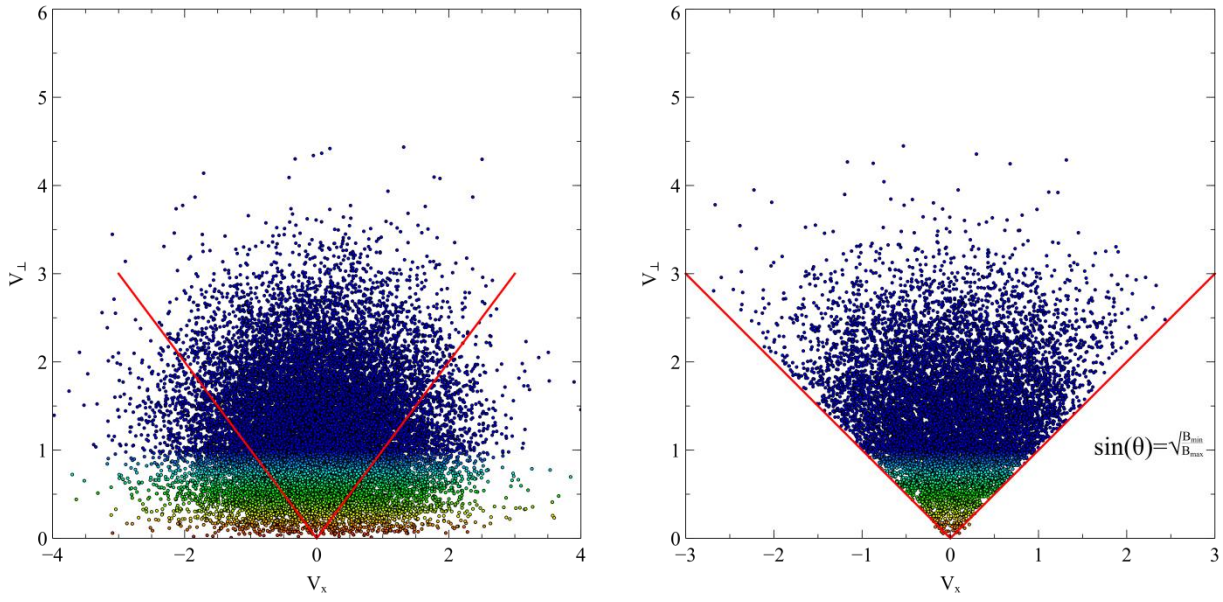

a) Initial state *b) Final State.*

Figure 6. Initial and final phase space distribution of an electron population trapped in a magnetic bottle. A the final state all the electron in the loss cone have been collected on the side walls.

III. Heating dynamic in the ECR regime

A. Heating Time at Resonance

As a first step to understand the heating regimes in the ECR thruster, we first consider an ideal situation where the plasma is uniform, in a constant static B field, with the resonance condition satisfied everywhere. This is a simplistic situation compared to what is found in the thruster, where the resonance zone is a surface, and electron will periodically cross this surface. This however can help us understand some basic features of the electron heating mechanism.

When the electrons reach the ECR surface in the thruster, the right-hand (circularly) polarized part of the electric field continuously accelerates them. Elastic collisions do not significantly change their kinetic energy but can induce a delay in the heating by changing the phase between the electron transverse velocity vector and the electric field. Inelastic collisions will lead to a loss of the threshold energy.

Using the cross sections shown in Figure 4, the mean time between collisions can be computed. In Figure 7 the collision times for the elastic process and the ionization are shown as a function of the electron energy. The heating curves for two different electric field magnitudes are also shown. In log coordinates, this heating curve has the form $T_{heat} \propto \sqrt{e_K}$. First, we notice that for a given number density, the ionization time is always larger than the elastic time, meaning that elastic collisions are more frequent. Second, there is an energy range between 100 eV and 200 eV where the collisions times for those two processes are roughly equal. For an electron population in

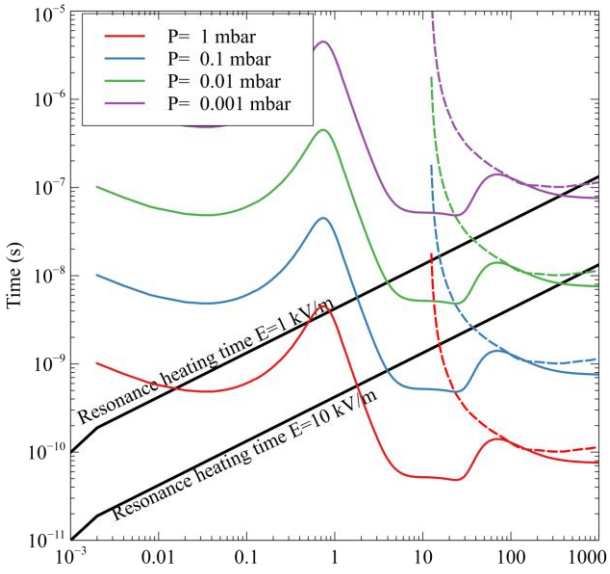

Figure 7. Time between collisions versus electron energy, for different Xenon pressures. The black curves show the time evolution of the electron energy at resonance, for two different electric field, with $f_{ECR} = 2.45\ GHz$

this energy range, one out of two collisions produces an ion-electron pair. For the electrons in the 12-20eV range, the elastic events are about one order of magnitude more frequent: only one event out of ten leads to the creation of an ion-electron pair.

Using this concept of heating curve, it is possible to derive a simple analytical model to find the collision frequencies for both elastic and ionization processes. An electron at the resonance condition will be continuously accelerated by the right-hand polarized electric field. Assuming a negligible initial thermal velocity, the electron velocity a time t is:

$$v(t) = \frac{eE_0 t}{m}$$

For a given collisional process, the probability to get a collision depends on the volume swept by the electron. This volume is:

$$V(t) = \int_0^t \sigma\big(\epsilon(t)\big) v(t) dt$$

Here, $\epsilon = \frac{1}{2} m v(t)^2$ is the kinetic energy of the electron. The probability for an electron to collide with an uniform background of neutrals is

$$P(t) = 1 - \exp\Big(-n_g V(t)\Big)$$

If the number of electrons in the sampled volume is N, then the number of electrons that have experienced a collision at a time t is:

$$N_c(t) = NP(t)$$

And the collision rate is:

$$\nu_c(t) = \frac{dN_c}{dt} = n_g \dot{V}(t) \exp\Big(-n_g V(t)\Big)$$

The result provided by this simple approach can be compared to the results obtained with the PIC/MCC code. We consider a 3D computational domain with periodic boundary conditions. The magnetic field is static, along the Ox direction. A uniform right-hand polarized electric field is applied in the simulation box such as the resonance condition is met. The box is initially loaded with a neutral plasma composed of electrons and Xenon ions. Two collisional processes are considered: elastic scattering and ionization. We assume the neutral background of neutral to be uniform at a prescribed number density n_g.

In Figure 8, the collision frequency rate obtained with the PIC simulation and the analytical approach is compared, showing an excellent agreement. As discussed above, when the electron energy is in the 100-200eV range, ionization events are as frequent as elastic collisions. Figure 9 shows the case of linearly polarized electric field with the same magnitude. Since a linear polarization can be decomposed in two circularly polarized wave with opposite direction and magnitudes twice as low, we should obtain the same collisions frequencies with the analytical model considering a field amplitude twice as low. Again, in this case the agreement is very good.

In the resonance region, the mean electron energy increases as the square of the time: $e_K \propto t^2$. This is true as long as the loss term due to the inelastic collisions remains small compared to the energy gain. In Figure 10, the transverse part of the electron energy closely follows this quadratic trend. Due to the elastic collisions, some electrons are scattered along the magnetic field axis and contribute to the heating in the parallel direction. When the pressure is increased, the contribution of inelastic losses and ionization lead to a saturation of the electron energy, as shown in Figure 11. The elastic collisions transfer the energy stored in the transverse part of the velocity to the axial part: the parallel kinetic energy, leading to a delayed heating of this degree of freedom compared to the transverse degrees of freedom.

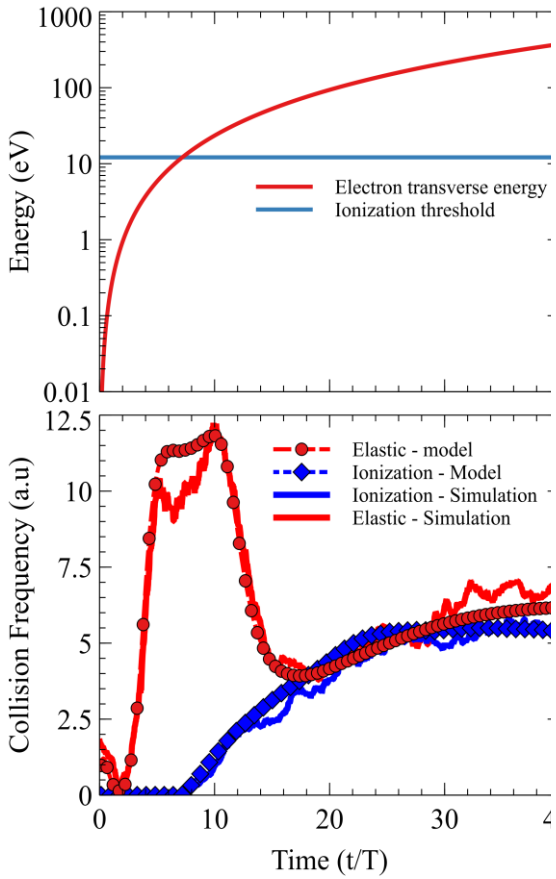

Figure 8. Collision Frequency as a function of time, from the PIC/MCC simulation and the analytical model. The top frame show the theoretical heating curve in red, with the threshold for ionization in blue. $T = 1/f_{ECR}$, Right-Hand polarized electric field of amplitude $E = 8000\ V/m$, $n_g = 2.5 \times 10^{19} m^{-3}$

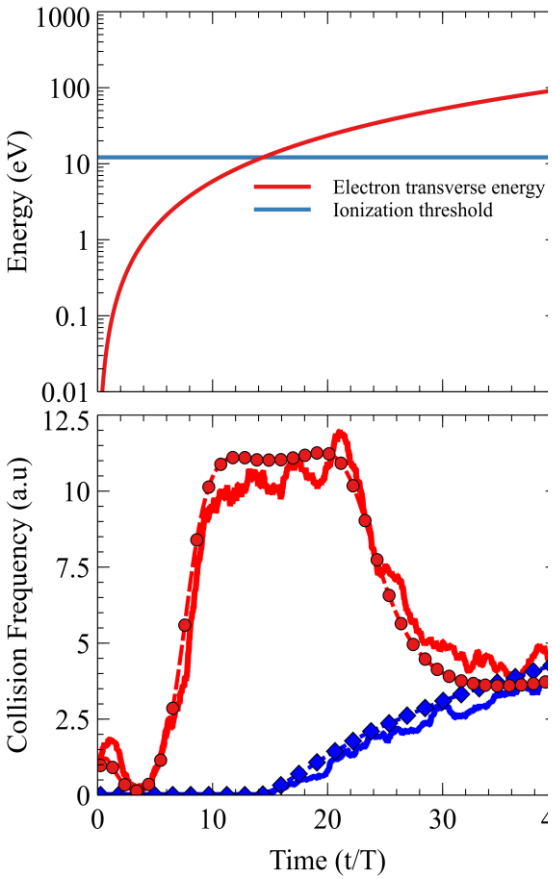

Figure 9. Collision Frequency as a function of time, from the PIC/MCC simulation and the analytical model. The top frame show the theoretical heating curve in red, with the threshold for ionization in blue. $T = 1/f_{ECR}$, Linearly polarized electric field of amplitude $E = 8000\ V/m$, $n_g = 2.5 \times 10^{19} m^{-3}$. Results with the analytical model are obtained using E= 4000 V/m

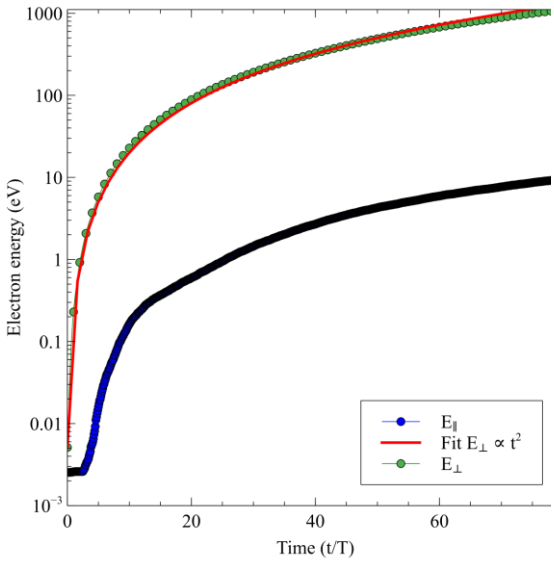

Figure 10. Parallel and perpendicular electron energy versus time .The red curve is the theoretical heating curve. E=4000 V/m, $n_g = 2.5 \times 10^{19} m^{-3}$

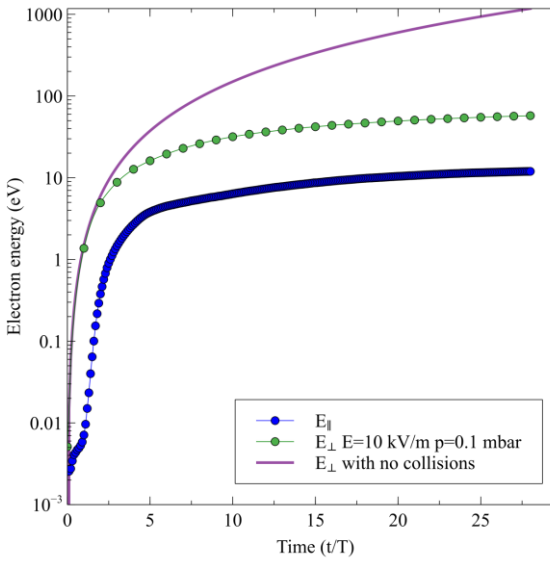

Figure 11. Parallel and perpendicular electron energy versus time .The red curve is the theoretical heating curve. E=10000 V/m, $n_g = 2.5 \times 10^{21} m^{-3}$

IV. Preliminary results of the 1.5D model of the thruster

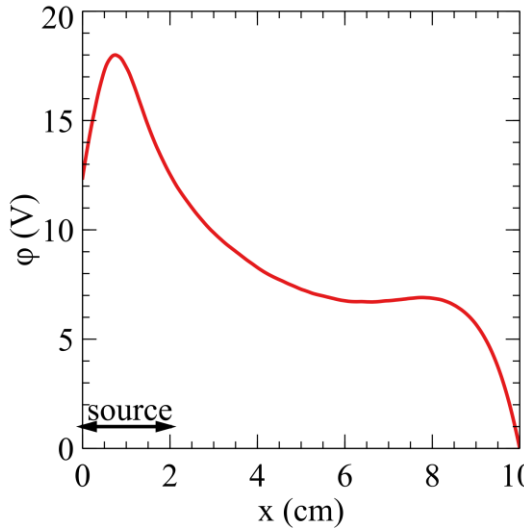

Figure 12. Steady state potential distribution in the magnetic field tube in fig.2. The electric field is applied in the source region only.

The above considerations leave behind several mechanisms that are important for the heating of the electrons. First, the magnetic field is monotonically decreasing in the source (see Figure 2). Therefore the resonance is a thin (Doppler-broadened) surface. Second, electrons can oscillate in the potential well of the expanding plasma. This means that they can cross several times the resonance zone, each time absorbing some power. Third, the hot electrons have a reduced confinement time in the source, since they are prone to escape the potential well in the far field plume, or, through elastic collision, can fall into the loss cone and be collected on the thruster backplate.

The model described in section II can be used to study the behavior of the ECR source and its plume in a magnetic field tube. Figure 12 and Figure 13 show preliminary results obtained at steady state with the model. Figure 12 shows that the thruster backplate collects ions to reach a steady state positive voltage that repels part of the ions produced in the source. The ions are then accelerated in the plume region before being collected by the vacuum chamber wall. The PIC/MCC models can provide the Electron Energy distribution function at various locations, as shown in Figure 13. Preliminary results indicate significant temperature anisotropy within the source. This is expected since most of the microwave power is transferred to the transverse kinetic energy of the electrons. This anisotropy is maintained in the plume, but the electrons with a high transverse kinetic energy are less confined and we can observe a depletion of these electrons. When moving downstream in the plume, we notice a shift of the EEDF toward the low energy, consistent with the voltage drop in the plume.

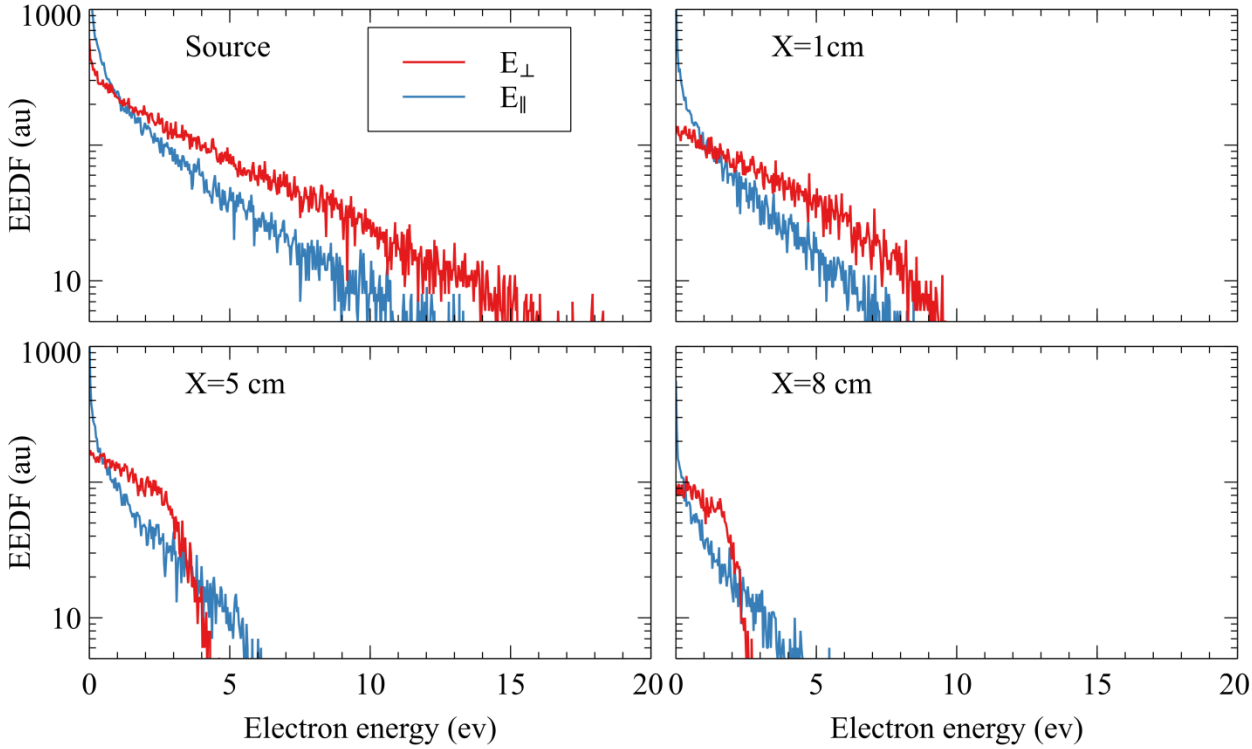

Figure 13. Electron Energy distribution function for the transverse and parallel energy at different location in the computational domain

V. Conclusion

In the frame of the development and the optimization of the ECRA thruster in the MINOTOR project, Onera is currently developing a dedicated PIC/MCC code whose goal is improve our understanding of the thruster, using massively parallel simulations. While the 3D Maxwell solver of the code is still in development, several features of the code are available and are being used to model the heating dynamic in the ECR source.

First, the heating regime has been investigated in a periodic 3D box for a plasma at the cyclotron resonance condition, with a uniform background of Xenon. At low pressure, the electron energy increases quadratically and can lead to an efficient ionization regime when the electron transverse energy reaches the 100-200 eV range. At higher pressure, the saturation due to inelastic collisions and the production of cold electron by ionization lead to a saturation of the electron energy.

Second, a 1.5D model of the thruster and its plume has been derived to model the motion of the electrons in the potential well. The preliminary result shows a significant temperature anisotropy in the source, and a gradual cooling of the electron in the plume. There, the transverse energy of the electron is depleted in the high energy region.

This model is currently being exploited to give some insight on the thruster operation regime and the heating dynamic in the source. It will provide basic information and enable parametric study the influence of several parameters such as the backplane material, the position of the ECR surface, the pressure, etc. These results will be compared to some experimental results. It will also be used to guide future EM-PIC simulation in 2D and 3D.

Acknowledgments

This work was made in the framework of project MINOTOR that has received funding from the European Union's Horizon 2020 research and innovation programme under grant agreement No 730028.

References

1. Packan, D. The 'MINOTOR' H2020 Project for ECR Thruster Development. in *35th International Electric Propulsion Conference* IEPC-2017-547 (2017).
2. Cannat, F. *et al*. Optimization of a coaxial electron cyclotron resonance plasma thruster with an analytical model. *Phys. Plasmas* **22,** 53503 (2015).
3. Bogdanov, E. A., Chirtsov, A. S. & Kudryavtsev, A. A. Fundamental Nonambipolarity of Electron Fluxes in 2D Plasmas. *Phys. Rev. Lett.* **106,** 195001 (2011).
4. Takao, Y., Koizumi, H., Komurasaki, K., Eriguchi, K. & Ono, K. Three-dimensional particle-in-cell simulation of a miniature plasma source for a microwave discharge ion thruster. *Plasma Sources Sci. Technol.* **23,** 64004 (2014).
5. Decyk, V. K. & Singh, T. V. Particle-in-Cell algorithms for emerging computer architectures. *Comput. Phys. Commun.* **185,** 708–719 (2014).
6. McEachran, R. P. & Stauffer, A. D. Momentum transfer cross sections for the heavy noble gases. *Eur. Phys. J. D* **68,** (2014).
7. Kinema Database on LXCAT. Available at: https://fr.lxcat.net/.
8. Birdsall, C. K. & Langdon, A. B. *Plasma Physics via Computer Simulation*. (IOP Publishing, 1991).
9. Joppich, W. & Mijalkovic, S. *Multigrid methods for process simulation*. (Springer Vienna, 2012). doi:10.1007/978-3-7091-9253-5